FERMILAB-PUB-19-260-CD-ND

Prepared for submission to JHEP

Energy calibration of the NEXT-White detector with 1% resolution near $Q_{\beta\beta}$ of ^{136}Xe

NEXT collaboration

J. Renner,[18] G. Díaz López,[20,15] P. Ferrario,[15,9,a] J.A. Hernando Morata,[20] M. Kekic,[18] G. Martínez-Lema,[18,20,b] F. Monrabal,[15] J.J. Gómez-Cadenas,[15,9,c] C. Adams,[2] V. Álvarez,[18] L. Arazi,[6] I.J. Arnquist,[19] C.D.R Azevedo,[4] K. Bailey,[2] F. Ballester,[21] J.M. Benlloch-Rodríguez,[18] F.I.G.M. Borges,[13] N. Byrnes,[3] S. Cárcel,[18] J.V. Carrión,[18] S. Cebrián,[22] E. Church,[19] C.A.N. Conde,[13] J. Díaz,[18] M. Diesburg,[5] J. Escada,[13] R. Esteve,[21] R. Felkai,[18] A.F.M. Fernandes,[12] L.M.P. Fernandes,[12] A.L. Ferreira,[4] E.D.C. Freitas,[12] J. Generowicz,[15] S. Ghosh,[11] A. Goldschmidt,[8] D. González-Díaz,[20] R. Guenette,[11] R.M. Gutiérrez,[10] J. Haefner,[11] K. Hafidi,[2] J. Hauptman,[1] C.A.O. Henriques,[12] P. Herrero,[15,18] V. Herrero,[21] Y. Ifergan,[6,7] S. Johnston,[2] B.J.P. Jones,[3] L. Labarga,[17] A. Laing,[3] P. Lebrun,[5] N. López-March,[18] M. Losada,[10] R.D.P. Mano,[12] J. Martín-Albo,[11] A. Martínez,[15] A.D. McDonald,[3] C.M.B. Monteiro,[12] F.J. Mora,[21] J. Muñoz Vidal,[18] P. Novella,[18] D.R. Nygren,[3,d] B. Palmeiro,[18] A. Para,[5] J. Pérez,[23] F. Psihas,[3] M. Querol,[18] J. Repond,[2] S. Riordan,[2] L. Ripoll,[16] Y. Rodríguez García,[10] J. Rodríguez,[21] L. Rogers,[3] B. Romeo,[15,23] C. Romo-Luque,[18] F.P. Santos,[13] J.M.F. dos Santos,[12] A. Simón,[6] C. Sofka,[14,f] M. Sorel,[18] T. Stiegler,[14] J.F. Toledo,[21] J. Torrent,[15] A. Usón,[18] J.F.C.A. Veloso,[4] R. Webb,[14] R. Weiss-Babai,[6,g] J.T. White,[14,h] K. Woodruff,[3] N. Yahlali[18]

[1] *Department of Physics and Astronomy, Iowa State University, 12 Physics Hall, Ames, IA 50011-3160, USA*

[2] *Argonne National Laboratory, Argonne, IL 60439, USA*

[3] *Department of Physics, University of Texas at Arlington, Arlington, TX 76019, USA*

[4] *Institute of Nanostructures, Nanomodelling and Nanofabrication (i3N), Universidade de Aveiro, Campus de Santiago, Aveiro, 3810-193, Portugal*

[5] *Fermi National Accelerator Laboratory, Batavia, IL 60510, USA*

[a] Corresponding author.

[b] Now at Weizmann Institute of Science, Israel.

[c] NEXT Co-spokesperson.

[d] NEXT Co-spokesperson.

[f] Now at University of Texas at Austin, USA.

[g] On leave from Soreq Nuclear Research Center, Yavneh, Israel.

[h] Deceased.

This document was prepared by [NEXT Collaboration] using the resources of the Fermi National Accelerator Laboratory (Fermilab), a U.S. Department of Energy, Office of Science, HEP User Facility. Fermilab is managed by Fermi Research Alliance, LLC (FRA), acting under Contract No. DE-AC02-07CH11359.

[6] *Nuclear Engineering Unit, Faculty of Engineering Sciences, Ben-Gurion University of the Negev, P.O.B. 653, Beer-Sheva, 8410501, Israel*

[7] *Nuclear Research Center Negev, Beer-Sheva, 84190, Israel*

[8] *Lawrence Berkeley National Laboratory (LBNL), 1 Cyclotron Road, Berkeley, CA 94720, USA*

[9] *Ikerbasque, Basque Foundation for Science, Bilbao, E-48013, Spain*

[10] *Centro de Investigación en Ciencias Básicas y Aplicadas, Universidad Antonio Nariño, Sede Circunvalar, Carretera 3 Este No. 47 A-15, Bogotá, Colombia*

[11] *Department of Physics, Harvard University, Cambridge, MA 02138, USA*

[12] *LIBPhys, Physics Department, University of Coimbra, Rua Larga, Coimbra, 3004-516, Portugal*

[13] *LIP, Department of Physics, University of Coimbra, Coimbra, 3004-516, Portugal*

[14] *Department of Physics and Astronomy, Texas A&M University, College Station, TX 77843-4242, USA*

[15] *Donostia International Physics Center (DIPC), Paseo Manuel Lardizabal, 4, Donostia-San Sebastian, E-20018, Spain*

[16] *Escola Politècnica Superior, Universitat de Girona, Av. Montilivi, s/n, Girona, E-17071, Spain*

[17] *Departamento de Física Teórica, Universidad Autónoma de Madrid, Campus de Cantoblanco, Madrid, E-28049, Spain*

[18] *Instituto de Física Corpuscular (IFIC), CSIC & Universitat de València, Calle Catedrático José Beltrán, 2, Paterna, E-46980, Spain*

[19] *Pacific Northwest National Laboratory (PNNL), Richland, WA 99352, USA*

[20] *Instituto Gallego de Física de Altas Energías, Univ. de Santiago de Compostela, Campus sur, Rúa Xosé María Suárez Núñez, s/n, Santiago de Compostela, E-15782, Spain*

[21] *Instituto de Instrumentación para Imagen Molecular (I3M), Centro Mixto CSIC - Universitat Politècnica de València, Camino de Vera s/n, Valencia, E-46022, Spain*

[22] *Laboratorio de Física Nuclear y Astropartículas, Universidad de Zaragoza, Calle Pedro Cerbuna, 12, Zaragoza, E-50009, Spain*

[23] *Laboratorio Subterráneo de Canfranc, Paseo de los Ayerbe s/n, Canfranc Estación, Huesca, E-22880, Spain*

E-mail: josren@uv.es

Abstract: Excellent energy resolution is one of the primary advantages of electroluminescent high pressure xenon TPCs, and searches for rare physics events such as neutrinoless double-beta decay ($\beta\beta0\nu$) require precise energy measurements. Using the NEXT-White detector, developed by the NEXT (Neutrino Experiment with a Xenon TPC) collaboration, we show for the first time that an energy resolution of 1% FWHM can be achieved at 2.6 MeV, establishing the present technology as the one with the best energy resolution of all xenon detectors for $\beta\beta0\nu$ searches.

Keywords: Neutrinoless double beta decay; TPC; high-pressure xenon chambers; Xenon; NEXT-100 experiment; energy resolution;

Contents

1 Introduction

Searches for neutrinoless double beta decay ($\beta\beta0\nu$), the observation of which would imply total lepton number violation and would show that neutrinos are Majorana particles [1–4], require excellent energy resolution to eliminate background events that occur at energies similar to the Q-value of the decay ($Q_{\beta\beta}$). The NEXT (Neutrino Experiment with a Xenon TPC) collaboration [5–8] intends to search for $\beta\beta0\nu$ using $\sim$ 100 kg of xenon enriched to 90% in the candidate isotope ^{136}Xe ($Q_{\beta\beta}$ = 2457.8 keV). In recent years, NEXT has developed and operated several gaseous xenon TPCs, including $\sim$ kg-scale detectors at Lawrence Berkeley National Lab (LBNL) and Instituto de Física Corpuscular (IFIC) [9, 10] and more recently the $\sim$ 5 kg-scale NEXT-White[1] at the Canfranc Underground Laboratory (LSC) in the Spanish Pyrenees [11].

Previous analyses [12] of the NEXT-White energy resolution using gammas from ^{137}Cs and ^{232}Th sources showed an extrapolated 1% FWHM resolution at $Q_{\beta\beta}$. The relatively low pressure (7.2 bar) at which those data were taken meant that electron tracks of events with energy near $Q_{\beta\beta}$ were not easily contained in the detector. Low statistics at the photopeak limited the highest energy at which a detailed analysis of energy resolution was performed to 1.6 MeV. More data has since been taken at a higher pressure (10.3 bar), and the results are reported in the present study. The experimental setup, similar to that of the previous study [12], is reviewed in section 2, and the analysis and obtained energy resolution are presented in section 3.

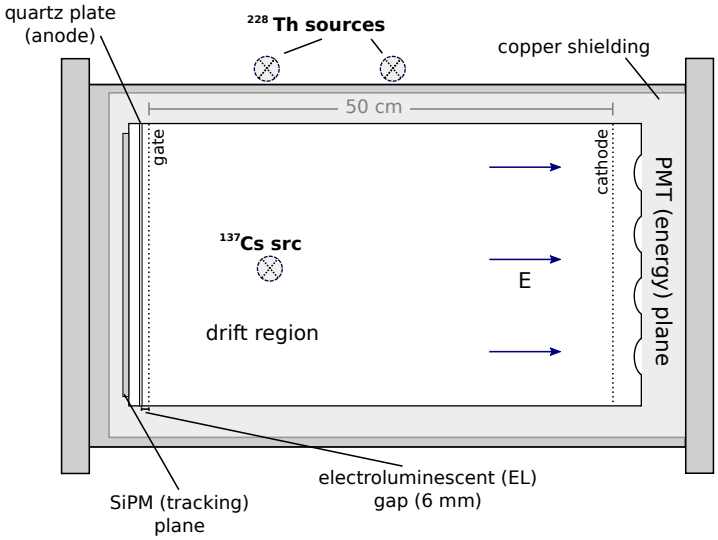

TPC parameter	Value
Pressure	∼10.3 bar *
E/p	1.3 kV cm^{-1} bar^{-1}
Drift field	415 V cm^{-1}
V_{cathode}	-30 kV
V_{gate}	-7.9 kV
Length	664.5 mm
Diameter	454 mm
EL gap	6 mm
Drift length	(530.3 ± 2.0) mm
Fiducial mass	3.3 kg

* The actual measured pressures for each run varied between 10.27-10.32 bar.

Figure 1: Experimental summary. (Left) Schematic of the main detector components and locations of the calibration sources (not drawn to scale). ^{137}Cs and ^{228}Th sources were placed in the lateral and top entrance ports of the pressure vessel respectively, and a second ^{228}Th source (the leftmost of the two) was placed directly on top of the vessel. (Right) NEXT-White operational parameters used in the present study.

2 Experimental setup

2.1 The NEXT-White electroluminescent TPC

The experimental setup is similar to that of the preceding study [12] and is summarized here. The detector NEXT-White is an electroluminescent (EL) time projection chamber (TPC) filled with xenon gas and equipped with photosensors to detect the UV light emitted in interactions occurring within the active volume. Charged particles deposit energy within the drift region, producing a track of ionized and excited xenon atoms. The UV light emitted in the relaxation of the excited xenon atoms, called primary scintillation or S1, is detected immediately and the ionized electrons are drifted toward a readout plane consisting of a narrow region of high electric field, the EL gap. In passing through the EL gap, the electrons are accelerated to energies high enough to further excite, but not ionize, the atoms of the xenon gas, leading to the production of an amount of secondary scintillation photons (S2) proportional to the number of electrons traversing the gap. This amplification process, electroluminescence, allows for gains on the order of 1000 photons per electron with significantly lower fluctuations than avalanche gain. In addition, the time elapsed between the observation of S1 and the arrival of S2 can be used to determine the axial (z) coordinate at which the interaction took place.

In NEXT-White (see Figure 1 and also [11]), the primary (S1) and secondary (S2) scintillation are detected by an array of 12 Hamamatsu R11410-10 photomultiplier tubes (PMTs), called the "energy plane" placed 130 mm from a transparent wire mesh cathode

[1] Named after our late mentor and friend Prof. James White.

Table 1: Summary of data analyzed in this study.

Run #	Duration	Avg. Rate	Triggers (low E)	Triggers (high E)	Avg. Lifetime (µs)
6346	25.0 h	42 Hz	3 485 555	313 761	3977
6347	23.6 h	41 Hz	3 250 612	304 948	4190
6348	23.5 h	41 Hz	3 210 597	307 397	4297
6349	23.8 h	41 Hz	3 248 563	311 204	4261
6351	23.9 h	41 Hz	3 260 929	311 951	4008
6352	24.6 h	41 Hz	3 345 650	321 545	3908
6365	24.4 h	41 Hz	3 300 055	318 662	3344
6482	26.7 h	41 Hz	3 257 113	739 668	3527
6483	24.7 h	41 Hz	3 006 991	684 718	3579
6484	24.4 h	41 Hz	2 959 826	681 687	3586
6485	20.3 h	41 Hz	2 453 528	566 984	3597

held at negative high voltage. An electric field is established in the drift region defined by the cathode and another transparent mesh (the "gate") located about 53 cm away. The EL region is defined by the mesh and a grounded quartz plate coated with indium tin oxide (ITO), placed 6 mm behind it. A grid (10 mm pitch) of 1792 SensL series-C silicon photomultipliers (SiPMs) is located behind the EL gap and measures the S2 scintillation, providing precise information on where the EL light was produced in (x, y). The active volume is shielded by an 60 mm thick ultra-pure inner copper shell, and the sensor planes are mounted on pure copper plates of thickness 120 mm. The sensor planes and active volume are enclosed in a pressure vessel constructed from the titanium-stabilized stainless steel alloy 316Ti. The vessel sits on top of a seismic table, and a lead shield that can be mechanically opened and closed surrounds the vessel. The vessel is connected to a gas system through which the xenon gas is continuously purified via the use of a hot getter. The entire experimental area, including gas system, electronics, pressure vessel, and seismic table, are stationed on an elevated tramex platform in the Laboratorio Subterráneo de Canfranc (LSC) in the Spanish Pyrenees.

2.2 Run configuration

As the goal of the present analysis was a detailed study of energy resolution, calibration sources were employed to yield energy peaks over a range of energies from several tens of keV up to and including $Q_{\beta\beta}$. ^{83m}Kr was injected into the xenon gas, providing a uniform distribution of 41.5 keV point-like energy depositions used to map out the geometric variations in the sensor responses and electron lifetime of the detector [13]. ^{137}Cs and ^{228}Th calibration sources were also placed as shown in Figure 1. The ^{137}Cs source provided 661.6 keV gamma rays, and ^{228}Th decays to ^{208}Tl which provides gammas of energy 2614.5 keV. In this study we focus on the energy peaks produced by interactions of these ^{137}Cs and ^{208}Tl gammas, and also the double-escape peak resulting from e^+e^- pair production interactions of the ^{208}Tl gamma in which the two 511 keV gammas escape. For the present

analysis, the acquisition trigger was split into a lower-energy trigger seeking the ^{83m}Kr events and a high-energy trigger aimed at capturing events with energy above $\sim$ 150 keV. A summary of the datasets analyzed is given in Table 1. For each run, the low-energy triggers were used to compute the lifetime and geometric correction maps used to correct the events acquired with the high-energy trigger. The average electron lifetime determined over the course of the analyzed runs is also shown in Figure 2.

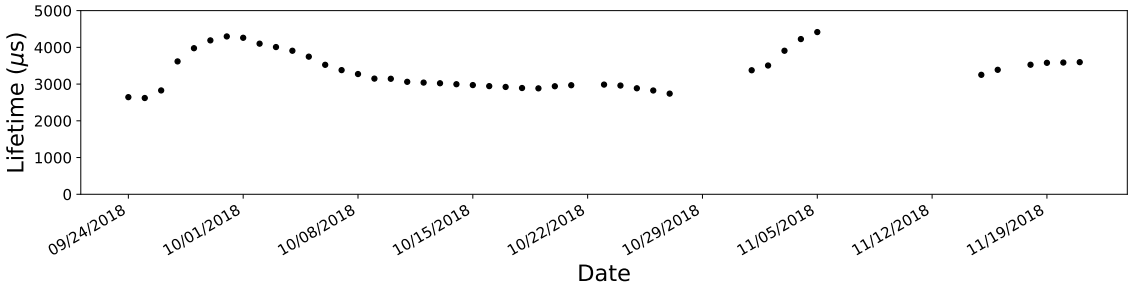

Figure 2: The average electron lifetime over the course of the analyzed runs determined using ^{83m}Kr events. The errors on the measurements are smaller than the size of the points. Though consistently above 2 ms, the electron lifetime was unstable and therefore was monitored and the corresponding corrections determined for each run.

3 Energy resolution

The signals from the SiPMs and PMTs were digitized in samples of width 1 µs and 25 ns respectively. Individual pulses in the energy plane waveform (summed over all PMTs, see Figure 3) were selected and classified as either S1 or S2. Events with a single identified S1 were selected, and the S2 peaks were divided into "slices" of width 2 µs.

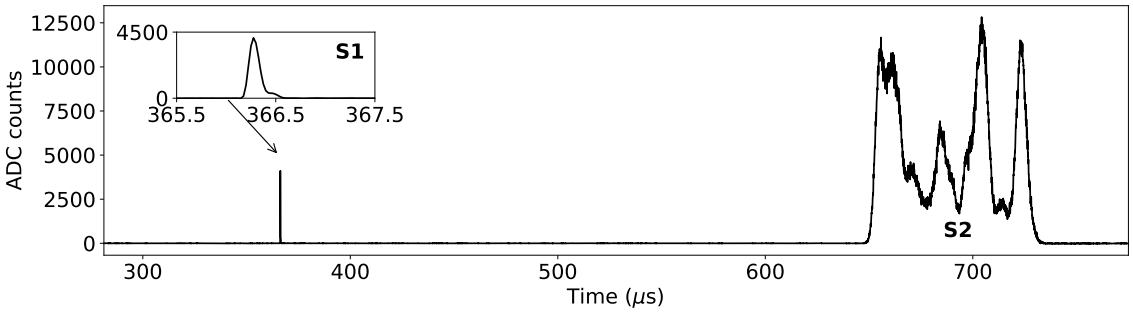

Figure 3: The acquired waveform, summed over all PMTs, for an event in the ^{208}Tl photopeak. Note that this particular event was identified to contain a single continuous track, as evident partially in the existence of a single long S2 pulse.

The pattern of light detected by the SiPMs of the tracking plane during the 2 µs interval of the slice was used to reconstruct the (x, y) location of the EL production, as done in [13], except multiple reconstructed positions sharing the energy E of a single slice were

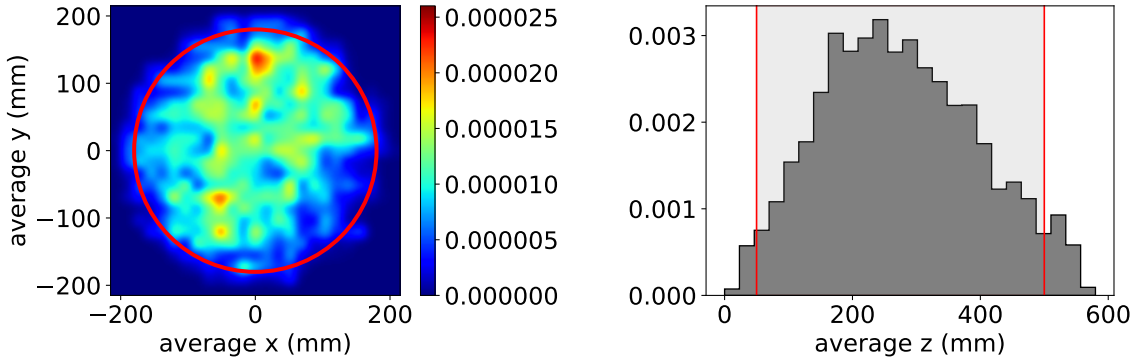

Figure 4: Normalized distributions in x-y (left) and z (right) of observed energy depositions for events in the 2615 keV ^{208}Tl photopeak (data from run 6485). The solid red lines show the fiducial cuts employed in this study which encompass nearly the entirety of the active volume. Note that the fiducial cuts are placed on all reconstructed energy depositions, rejecting an event if one or more depositions occurred outside the cut.

possible, to allow for reconstruction of long tracks that may double-back on themselves. The time elapsed since the S1 pulse was used to determine the z coordinate of each slice, and the energies E of the reconstructed depositions (x, y, z, E) were then multiplied by two correction factors: one accounting for the geometrical (x, y) dependence of the light collection over the EL plane, and another accounting for losses due to the finite electron lifetime caused by attachment to impurities. This second factor depended on the drift length (z-coordinate) and the location in the EL plane (x, y), as the electron lifetime also varied in (x, y). Once fully reconstructed, fiducial cuts were made on each event as detailed in Figure 4.

A final correction was applied for an empirically observed dependence on the track orientation. The origin of this dependence, whereby the measured energy of an event decreases with increasing axial (z) extent of the track, is still under study. However, we find it can be effectively corrected, as follows. The z-extent Δz is defined as the difference between the maximum and minimum z-coordinates of all reconstructed slices in the event. The effect is shown in Figure 5 along with the resolution obtained for each of the three peaks (662 keV, 1592 keV, and 2615 keV) after correcting for the effect using the average of the normalized slopes determined by a linear fit to each distribution,

$$E_{\text{corrected}} = \frac{E}{1 - (m/b)\Delta z}, \tag{3.1}$$

where m and b are the slope and intercept of the linear fit for Δz in mm. Note that the linear fits were performed on the events between the dashed lines. Reasonable variations on the positioning of these lines gave an error of approximately 0.2×10^{-4} for each computed slope in addition to the statistical errors shown on the distributions in Figure 5 (left). In determining the slopes (m/b) and in the subsequent determination of energy resolution, all events were required to have z-lengths in the ranges shown on the x-axes of the 2D distributions. Furthermore, in order to avoid complications in the spectrum

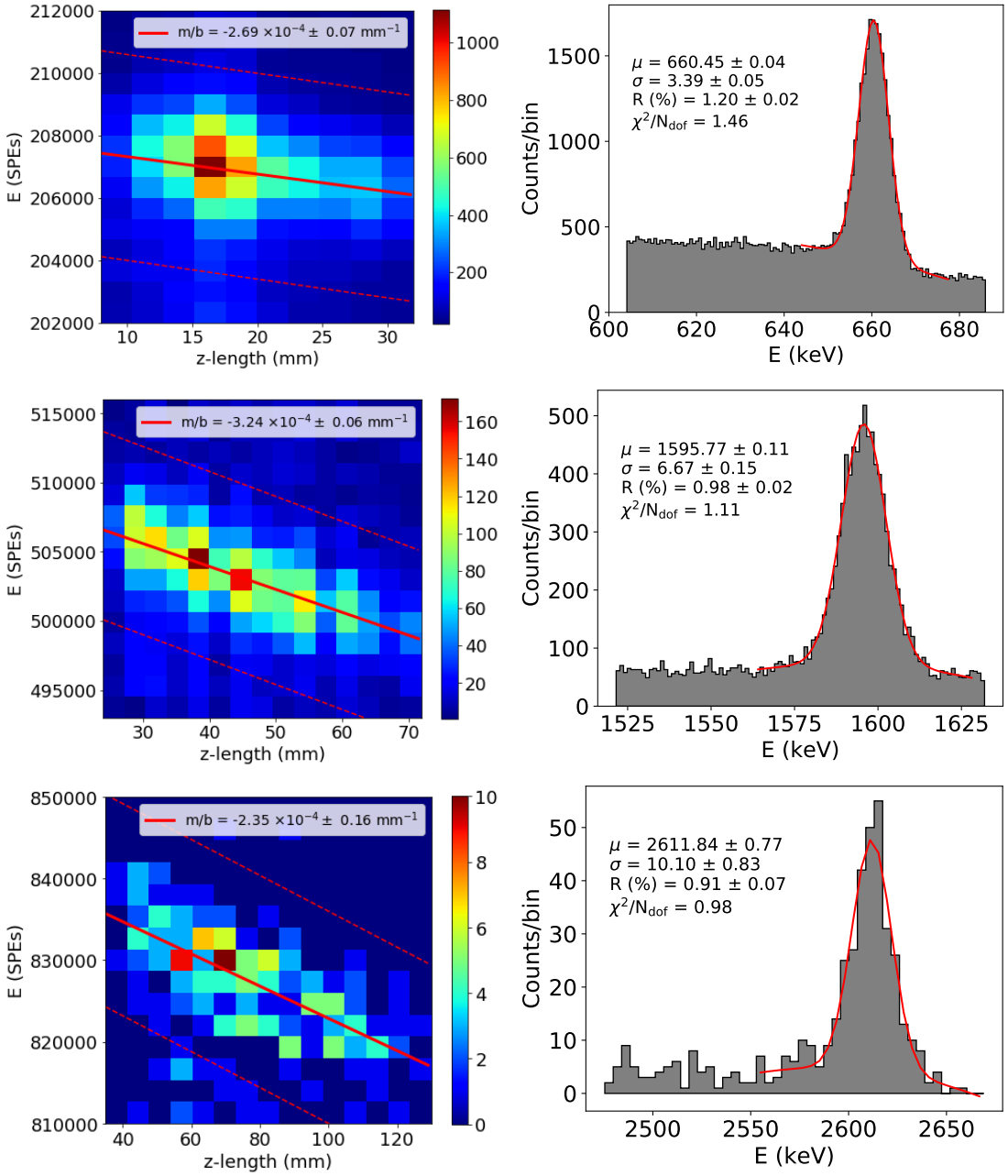

Figure 5: Fits to the dependence of energy on track length in the axial dimension (left), and the resulting energy spectra of three energy peaks after application of all corrections, including a linear correction to the energy (equation 3.1) corresponding to the average value of $(m/b) = 2.76 \times 10^{-4}$ obtained from the 3 fits (right).

caused by interactions producing isolated secondary depositions such as Compton scattering, bremsstrahlung, and the emission of characteristic x-rays, all events were required to have been reconstructed as single continuous tracks. To demonstrate the validity of the correction over time, data (see table 1) from runs 6346, 6347, 6348, 6349, and 6351 were used to

determine the slopes (m/b), and the remaining data, runs 6352, 6365, 6482, 6483, 6484, and 6485, were used to evaluate the energy resolution.

Each peak was fitted to the sum of a Gaussian and a 2nd-order polynomial to account for the surrounding distribution of background events, and the resolution was computed using the width of the Gaussian. The obtained resolutions are: $1.20 \pm 0.02\%$ FWHM at 662 keV; $0.98 \pm 0.03\%$ FWHM at 1592 keV; and $0.91 \pm 0.12\%$ FWHM at 2615 keV. The total errors are estimated in each case based on the statistical errors of the fits (shown on the histograms in Figure 5) and systematic effects including variations in the range of events included in the fit and (systematic) errors in the correction for the axial length effect. The energy conversion from detected photoelectrons to keV was determined (after application of all corrections) using a quadratic fit to the means of the three peaks of interest (662 keV, 1592 keV, 2615 keV) and the 29.7 keV K-α xenon x-ray peak. The x-rays had energies too low to be triggered on as individual events, but their energies were visible by examining the spectrum of isolated energy depositions within all events, which included small depositions due to xenon x-rays that traveled away from the main track before interacting.

The energy spectrum of high-energy triggers in the full active volume is shown in Figure 6 after applying all corrections described in section 3. Unlike in the previous study [12], the ^{208}Tl photopeak at 2615 keV (near $Q_{\beta\beta}$) is clearly resolved. The squared resolution is shown vs. the inverse energy in Figure 7 for the three energy peaks studied and fit to a line, $R^2 = a/E + b$, where $a = 548.52 \pm 82.15$ and $b = 0.62 \pm 0.10$. The presence of a constant term in the resolution shows that detector-specific systematic effects have not been completely eliminated by the corrections, and there is still room for further improvement. Nevertheless, these results demonstrate that excellent energy resolution is obtainable throughout the entire fiducial volume once correction for the axial length effect is made. Unlike corrections for electron lifetime, the correction for the axial length effect was relatively stable throughout the time ($\sim$ 8 weeks) over which the data presented in this study was taken. Further explanation of the axial length effect is given in appendix A.

4 Summary

Energy resolution in the NEXT-White TPC has been further studied, and a resolution better than 1% FWHM is shown to be obtainable at 2615 keV, as predicted in the preceding study [12]. This resolution was obtained over nearly the entire active volume, demonstrating the effectiveness of the continuous ^{83m}Kr-based calibration procedure implemented to correct for geometric and lifetime effects, and improved slightly with more restrictive fiducial cuts. Further study is required to understand the observed "axial length effect" in which the measured energy of extended tracks decreases with increasing track length in the axial (drift) direction. However, as HPXe TPCs provide detailed energy and topological information for each event, such effects can be remedied through careful calibration, and the outstanding resolution obtained highlights the strong potential of this detector technology to host a sensitive $0\nu\beta\beta$ search in which good energy resolution is essential.

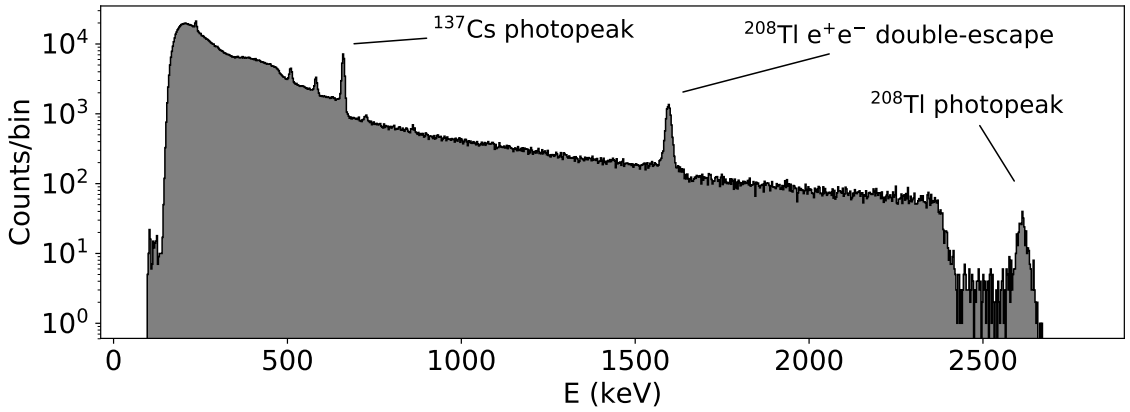

Figure 6: The full energy spectrum for events with energies greater than $\sim$ 150 keV. Corrections for electron lifetime and geometrical effects were applied to all events, as well as a correction for the described axial length effect (see section 3) corresponding to $(m/b) = 2.76 \times 10^{-4}$. In addition to the three lines examined in detail in this study, lines are also present due to other gammas from the ^{228}Th decay chain: at 238 keV (from ^{212}Pb $\rightarrow$ ^{212}Bi decay), 511 keV (e$^+$e$^-$ annihilation, with some contribution from ^{208}Tl $\rightarrow$ ^{208}Pb decay), 583 keV (^{208}Tl $\rightarrow$ ^{208}Pb decay), 727 keV (^{212}Bi $\rightarrow$ ^{212}Po decay), and 860 keV (^{208}Tl $\rightarrow$ ^{208}Pb decay).

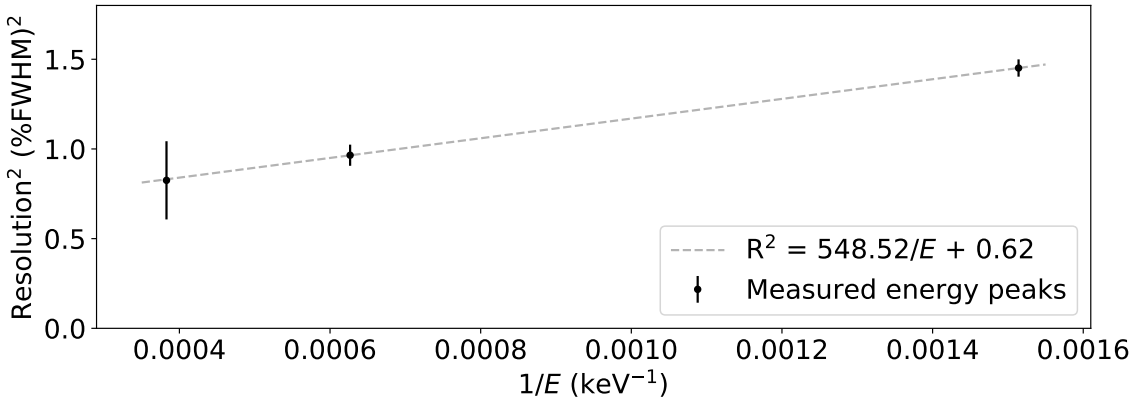

Figure 7: Squared energy resolution plotted against $1/E$. The measured points were fit to the functional form $R^2 = a/E + b$, with $a = 548.52 \pm 82.15$ and $b = 0.62 \pm 0.10$.

Acknowledgments

The NEXT Collaboration acknowledges support from the following agencies and institutions: the European Research Council (ERC) under the Advanced Grant 339787-NEXT; the European Union's Framework Programme for Research and Innovation Horizon 2020 (2014-2020) under the Marie Skłodowska-Curie Grant Agreements No. 674896, 690575 and 740055; the Ministerio de Economía y Competitividad and the Ministerio de Ciencia, Innovación y Universidades of Spain under grants FIS2014-53371-C04, RTI2018-095979, the Severo Ochoa

Program SEV-2014-0398 and the María de Maetzu Program MDM-2016-0692; the GVA of Spain under grants PROMETEO/2016/120 and SEJI/2017/011; the Portuguese FCT under project PTDC/FIS-NUC/2525/2014, under project UID/FIS/04559/2013 to fund the activities of LIBPhys, and under grants PD/BD/105921/2014, SFRH/BPD/109180/2015 and SFRH/BPD/76842/2011; the U.S. Department of Energy under contracts number DE-AC02-06CH11357 (Argonne National Laboratory), DE-AC02-07CH11359 (Fermi National Accelerator Laboratory), DE-FG02-13ER42020 (Texas A&M) and DE-SC0019223 / DE-SC0019054 (University of Texas at Arlington); and the University of Texas at Arlington. DGD acknowledges Ramon y Cajal program (Spain) under contract number RYC-2015-18820. We also warmly acknowledge the Laboratori Nazionali del Gran Sasso (LNGS) and the Dark Side collaboration for their help with TPB coating of various parts of the NEXT-White TPC. Finally, we are grateful to the Laboratorio Subterráneo de Canfranc for hosting and supporting the NEXT experiment.

References

[1] J. Schechter and J. W. F. Valle, *Neutrinoless Double beta Decay in SU(2)× U(1) Theories*, *Phys. Rev. D* **25** (1982) 2951.

[2] J. Gómez-Cadenas, J. Martín-Albo, J. Munoz Vidal, and C. Pena-Garay, *Discovery potential of xenon-based neutrinoless double beta decay experiments in light of small angular scale CMB observations*, *JCAP* **1303** (2013) 043, [arXiv:1301.2901].

[3] F. T. Avignone III, S. R. Elliott, and J. Engel, *Double beta decay, Majorana neutrinos, and neutrino mass*, *Rev. Mod. Phys.* **80** (2008) 481, [arXiv:0708.1033].

[4] J. J. Gómez Cadenas, J. Martín-Albo, M. Mezzetto, F. Monrabal, and M. Sorel, *The Search for Neutrinoless Double Beta Decay*, *Riv. Nuovo Cim* **35** (2012), no. 3 29–98.

[5] **NEXT** Collaboration, V. Álvarez et al., *The NEXT-100 experiment for neutrinoless double beta decay searches (Conceptual Design Report)*, arXiv:1106.3630.

[6] **NEXT** Collaboration, V. Álvarez et al., *NEXT-100 Technical Design Report (TDR): Executive Summary*, *JINST* **7** (2012) T06001, [arXiv:1202.0721].

[7] **NEXT** Collaboration, J. J. Gomez-Cadenas et al., *Present status and future perspectives of the NEXT experiment*, *Adv. High Energy Phys.* **2014** (2014) 907067, [arXiv:1307.3914].

[8] **NEXT** Collaboration, J. Martín-Albo et al., *Sensitivity of NEXT-100 to Neutrinoless Double Beta Decay*, *JHEP* **05** (2016) 159, [arXiv:1511.09246].

[9] **NEXT** Collaboration, V. Álvarez et al., *Near-Intrinsic Energy Resolution for 30 to 662 keV Gamma Rays in a High Pressure Xenon Electroluminescent TPC*, *Nucl. Instrum. Meth.* **A708** (2012) 101–114, [arXiv:1211.4474].

[10] **NEXT** Collaboration, V. Álvarez et al., *Initial results of NEXT-DEMO, a large-scale prototype of the NEXT-100 experiment*, *JINST* **8** (2013) P04002, [arXiv:1211.4838].

[11] **NEXT** Collaboration, F. Monrabal et al., *The Next White (NEW) Detector*, *JINST* **13** (2018) P12010, [arXiv:1804.02409].

[12] **NEXT** Collaboration, J. Renner et al., *Initial results on energy resolution of the NEXT-White detector*, *JINST* **13** (2018) P10020, [arXiv:1808.01804].

[13] **NEXT** Collaboration, G. Martínez-Lema et al., *Calibration of the NEXT-White detector using* ^{83m}Kr *decays*, *JINST* **13** (2018) P10014, [arXiv:1804.01780].

A The axial length effect

The origin of the axial length effect is still under detailed study. However, a number of possible origins have already been discarded:

- **PMT saturation / baseline shift:** due to the AC-coupled PMT readout scheme used in NEXT-White [11], all PMT waveforms must be passed through a deconvolution algorithm to remove distortions introduced by high-pass filtering before beginning physics analysis. It was found that if the response of a PMT saturates, the deconvolution may lead to a shifted baseline which could lead to an error in the signal integration (energy) dependent on the length of integration in time (z). However, the effect was found to persist even after lowering PMT gains, ensuring no saturation, and it was confirmed that any shift in baseline present after the deconvolution was not significant enough to account for the effect.

- **Recombination:** as the electrons are drifted in the z-dimension towards the EL plane, it was proposed that tracks extended in this dimension present a greater opportunity for drifting electrons to encounter neighboring ions and recombine. Since these electrons would not arrive at the EL plane and produce light, this would lead to a lower energy measurement. However, basic simulations concluded that the recombination capture radius would need to be on the order of several tens of µm to explain the effect, an unphysically large sphere of influence for a single ion. In addition, electron-ion recombination would lead to scintillation light that should be observable during a time interval beginning after primary scintillation and ending after an amount of time required to drift the electrons over the entire track length in z. For ^{208}Tl photopeak events (see Figure 5, bottom), this would be about 120 µs, and integrating over this interval after the arrival of S1 for many such events, no evidence of the expected light was observed.

- **Variations in electron lifetime:** as the measured electron lifetime in NEXT-White is known to vary with location in the detector, there has been concern that small errors in the computation of the lifetime were giving rise to the observed effect when applied over long tracks. However, even after correcting Cs-photopeak events using a single average position (assuming pointlike tracks), the effect could still be observed by making a tight cut on average radius (effectively eliminating the error due to response variations in the xy-plane by considering only events that did not require significant xy correction).

- **Light emitted from the SiPMs:** the effect is also seen in the integrated charge of the SiPMs, and in fact is more dramatic (the normalized slopes m/b analogous to those shown in Figure 5 are greater in magnitude). Therefore it was proposed that the

SiPMs may be emitting additional light in a nonlinear manner during the production of EL. However, even after turning off the SiPM plane and using only information from the PMT plane for a less-precise xy reconstruction, the effect was still observed.

Several explanations for the effect have not yet been investigated in detail:

- **"Charge-up" effect at the EL plane:** an electron crossing the EL gap may, at least locally, alter the electric field seen by the next electron crossing the gap for some amount of time. If this were to make the average gain somewhat dependent on track orientation - whether the electrons cross the gap more in "series" (more extended in z) or in "parallel" (more extended in xy) - this could give rise to the observed effect.
- **Attachment to ionized impurities in the EL gap:** The wavelength shifter tetraphenyl butadiene (TPB) is deposited on several components in NEXT-White including the quartz plate just behind the EL region, to shift the VUV scintillation produced by xenon to visible light that can be detected by the photosensors (the SiPMs are not VUV sensitive, and the PMTs are placed inside enclosures behind sapphire windows, which do not transmit VUV light, to shield them from the high pressure environment inside the detector). If the photons produced in electroluminescence are capable of photoionizing the TPB, the resulting ions would be drifted across the EL region, possibly capturing some of the electrons that arrived at later times before completely traversing the EL gap and thereby reducing the observed energy of the event.

The observed effect could also be a result of a nonlinearity in the light production process caused by some other internal component. Further investigation in future runs with NEXT-White, possibly involving alterations of the internal hardware and/or running systematically at different EL gains, will be necessary to understand this effect. Nevertheless, excellent resolution has been obtained due to the properties of HPXe TPCs, such as simultaneous energy and 3D position measurements, which allow for detailed calibration.